A novel recognition and classification approach for motor imagery based on spatio-temporal features

Renjie Lv, Wenwen Chang, Guanghui Yan,Wenchao Nie, Lei Zheng, Bin Guo, and Muhammad Tariq Sadiq

***Abstract*— Motor imagery, as a paradigm of brain-machine interfaces, holds vast potential in the field of medical rehabilitation. Addressing the challenges posed by the non-stationarity and low signal-to-noise ratio of EEG signals, the effective extraction of features from motor imagery signals for accurate recognition stands as a key focus in motor imagery brain-machine interface technology. This paper proposes a motor imagery EEG signal classification model that combines functional brain networks with graph convolutional networks. First, functional brain networks are constructed using different brain functional connectivity metrics, and graph theory features are calculated to deeply analyze the characteristics of brain networks under different motor tasks. Then, the constructed functional brain networks are combined with graph convolutional networks for the classification and recognition of motor imagery tasks. The analysis based on brain functional connectivity reveals that the functional connectivity strength during the both fists task is significantly higher than that of other motor imagery tasks, and the functional connectivity strength during actual movement is generally superior to that of motor imagery tasks. In experiments conducted on the Physionet public dataset, the proposed model achieved a classification accuracy of 88.39% under multi-subject conditions, significantly outperforming traditional methods. Under single-subject conditions, the model effectively addressed the issue of individual variability, achieving an average classification accuracy of 99.31%. These results indicate that the proposed model not only exhibits excellent performance in the classification of motor imagery tasks but also provides new insights into the functional connectivity characteristics of different motor tasks and their corresponding brain regions.**

***Index Terms*— Brain-computer Interface (BCI), Functional Brain Networks, Graph Theory, graph convolutional networks (GCN), Motor Imagery (MI).**

This work was supported in part by the National Natural Science Foundation of China under grant 62366028 and grant 62466032, in part by the Major Science and Technology Projects of Gansu Province under grant 23ZDFA012, in part by the Young Doctoral Program of Gansu Department of Education under grant 2023QB-038, in part by the Science and Technology Program of Gansu Province under grant 24JRRA256.(Corresponding author: Wenwen Chang.)

Renjie Lv, Wenwen Chang, Guanghui Yan, Wenchao Nie, and Lei Zhen are with the School of Electronic and Information Engineering, Lanzhou Jiaotong University, Lanzhou 730070, China (e-mail: lvrenjie2022@163.com; e-mail:changww2013@126.com; e-mail:yanguanghui@mail.lzjtu.cn; e-mail:nwc13919186880@126.com; e-mail:zl13383560179@163.com).

Bin Guo is with the School of Computer Science, Northwestern Polytechnical University, Xi'an 710129, China (e-mail: guobin.keio@gmail.com).

Muhammad Tariq Sadiq is with the School of Computer Science and Electronic Engineering, University of Essex, United Kingdom (e-mail: m.t.sadiq@essex.ac.uk).

I. Introduction

BRAIN-COMPUTER interface systems, serving as a direct channel for the interaction between the brain and the external environment, enable communication between the human brain and external devices [1]. As a novel form of human-machine interaction, BCI has gained significant attention from researchers in recent years. Initially applied in the field of medical rehabilitation, BCI systems assist stroke survivors and paralyzed patients in communicating with the external world, facilitating the use of wheelchairs, prosthetics, robotic arms, and more for individuals with impaired limb functions [2]. Currently, with the continuous development of brain science and signal processing, BCI is also widely used in robot control, military, education, entertainment, and other fields [3].

BCI systems can be categorized as invasive, non-invasive, and semi-invasive depending on the method of acquisition [4]. Invasive and semi-invasive methods are used for signal acquisition by surgically implanting electrodes in the cerebral cortex or between the scalp and the cerebral cortex [5]. Although the signals acquired by invasive and non-invasive methods are of higher quality, the surgical risks are higher and portability is poor. The non-invasive type only needs to acquire and process signals directly on the surface of the cerebral cortex through relevant equipment, without the need for surgical intervention, and has become a hot direction of BCI research [6]. Commonly used non-invasive signals include scalp electroencephalography (EEG), functional near-infrared spectroscopy [7] (fNIRS), and functional magnetic resonance imaging [8] (fMRI), etc., among which EEG is the most common. EEG is usually used by a head-mounted EEG cap to acquire signals on the scalp, which is characterized by high temporal resolution and portability [9], etc. The EEG brain-computer interface system can be further divided into P300 brain-computer interface, steady-state visual evoked potentials, and motor imagery. Motor imagery brain-computer interfaces usually do not require additional stimuli to induce EEG potential activity and do not require additional assistive devices, making them easier to use and more promising for users and researchers [10]. However, due to the non-stationary and low signal-to-noise ratio characteristics of EEG signals, it is a challenging problem to improve the classification and recognition accuracy of motor imagery brain-computer interface systems [11].

In recent years, an increasing number of researchers have employed graph theory and complex network methods to decode EEG signals, treating the brain as a complex network. Drawing inspiration from graph theory, they have proposed functional brain networks to depict the connectivity between brain regions during tasks involving motor imagery [12]–[14]. However, functional brain networks, being a form of spatially discrete data, are often challenging to process using traditional machine learning algorithms and convolutional neural network (CNN) approaches. Graph neural network algorithms, on the other hand, prove effective in extracting spatial features from functional brain networks [15]. Motivated by the insights from functional brain networks and graph neural networks, we leverage various brain functional connectivity metrics to construct spatial features and employ graph neural networks for classification and recognition tasks.

In summary, this paper makes the following contributions:

1) : Designing a targeted Functional brain network-GCN model to effectively extract time and space domain features while quadruple classifying real movement and motor imagery tasks.

2) : Utilizing distinct brain functional connectivity metrics and the methods of complex networks in graph theory, we examine the connectivity relationships among various brain regions during both actual movement and motor imagery tasks, as well as across different motor tasks.

3) : The method in this paper obtains better classification performance and has good robustness compared with other classification models.

The remaining parts of this paper are organized as follows: Section II provides a brief overview of related research in the field. Section III details the experimental methods and introduces the concepts of brain functional connectivity measures and graph neural networks. Section IV introduces the data used in the study, discusses the data preprocessing steps, analyzes brain functional connectivity using graph theory and complex network metrics, and presents the performance of our proposed model. Section V discusses the experimental results, further validating the model's performance and comparing it with other classification methods. Section VI concludes the paper.

II. Related work

The classification of motor imagery tasks based on different feature extraction algorithms is usually divided into traditional machine learning methods and deep learning methods. Traditional machine learning-based motor imagery classification methods mainly consist of preprocessing, feature extraction, and classification recognition steps [16]. Firstly, the brainwave signals are preprocessed, primarily involving filtering and artifact removal. Secondly, feature extraction is performed on the preprocessed data, with methods mainly including wavelet transform based on time-frequency features and common spatial pattern algorithms based on spatial domain features, among which CSP and its improved algorithms are widely applied. Finally, traditional machine learning algorithms such as LDA, KNN, SVM, and RF are used for classification recognition [17]–[22]. However, traditional machine learning methods often require preprocessing, which not only consumes time but also requires personal experience and prior knowledge. Relying solely on personal experience and prior knowledge is difficult to apply to various scenarios, and it also results in poor robustness, ultimately leading to lower accuracy in MI signal recognition.

With the development of deep learning in fields such as computer vision and language recognition, many researchers have turned their attention to utilizing deep learning algorithms for the processing of electroencephalogram (EEG) signals [23]–[31]. Deep learning methods can directly handle raw EEG signals and automatically extract features and classify them, saving time while also improving model classification accuracy. The work by Schirrmeister et al. [23]and the EEGNet team [24] has made significant contributions to the spatiotemporal decoding of EEG signals. By introducing models with temporal and spatial convolutional substructures such as Shallow ConvNet, Deep ConvNet, and Hybrid ConvNet, these studies have demonstrated the potential of deep learning methods in this field. Although the improvement in accuracy may not be significant compared to traditional methods like FBCSP, this demonstrates the effectiveness of deep learning methods comparable to traditional approaches. Specifically, EEGNet has proposed a compact convolutional neural network model that conducts deep convolution along both temporal and spatial dimensions, suitable for decoding various brain-computer interface paradigms. These CNN-based models have brought new ideas and tools to the field of brain-computer interfaces, inspiring many excellent research endeavors. For example, Altaheri et al. [25] proposed a Dynamic Attention Time Convolutional Network (D-ATCNet) for decoding MI signals based on EEG, employing dynamic convolution (Dyconv) to represent temporal correlations and adding multi-level attention to enhance MI classification performance with relatively fewer parameters. Hwang et al. [26] proposed a multiband FBCSP and LSTM classification algorithm using sliding windows and FBCSP based on overlapping frequency bands to extract features for each window, overcoming dependency on frequency bands, and using LSTM for temporal classification, achieving good classification performance in four-class tasks. Jia et al. [27] proposed a Multi-Branch Multi-Scale Convolutional Neural Network (MMCNN) that addresses individual differences by extracting and integrating features at different scales, improving the accuracy of MI-EEG classification. Hou et al. [28] proposed a motion imagination classification method combining ESI technology with CNN, using boundary element method and weighted minimum norm estimation to solve forward and backward processes respectively, extracting MI-EEG features using Morlet wavelet analysis in regions of interest, achieving an average accuracy of 94.5% on the Physionet public dataset. The shallow convolutional neural network model proposed by Dose et al. [29] and the algorithm combining CNN and discrete wavelet transform proposed by Yang et al. [30] have made significant progress in decoding spatiotemporal features. In addition, Li et al. [31] proposed a neural network feature fusion algorithm that utilizes CNN and LSTM for spatial and temporal feature extraction, achieving

satisfactory average accuracy. These research works enrich the methodology of brain-computer interfaces and provide new ideas and tools for solving complex EEG signal decoding problems. Although many studies consider both temporal and frequency domain features when processing EEG signals, consideration for spatial domain features is often insufficient. Spatial domain features include the relative positions and intrinsic relationships between electrodes, which are crucial for accurately decoding EEG signals. While some current methods attempt to consider spatial features, they often still rely on convolutional operations along both temporal and spatial dimensions, and CNNs may not fully capture the complex spatial features of EEG signals. This limitation in handling EEG data may affect model performance.

To further explore better integration of spatial domain features, some researchers have adopted graph-theoretical approaches to decode electroencephalography (EEG) signals, treating the brain as a complex network. They propose functional brain networks to describe the connectivity between different brain regions during motor imagery tasks. Early research primarily focused on constructing functional connectivity maps using simple correlations or mutual information [32]–[34], and analyzing their basic properties such as node degree, clustering coefficient, and path length. With advances in research methods and technology, researchers began to adopt more sophisticated approaches to construct brain functional connectivity maps, such as using phase synchronization and Granger causality to more accurately capture the dynamic connections between brain regions [35], [36]. During this stage, graph theory features such as modularity and betweenness centrality were widely applied to identify global and local characteristics of brain networks, and were used in tasks such as brain disease diagnosis and cognitive state assessment. In recent years, the combination of graph theory methods with advanced techniques such as machine learning, deep learning, and complex network analysis has further enhanced the ability to analyze EEG signals [37], [38], [57]. However, traditional deep learning models such as CNNs and LSTMs often have limitations when extracting features from brain networks, which are non-Euclidean spatial data. To address this issue, some researchers have introduced Graph Convolutional Networks (GCNs) to handle non-Euclidean spatial data, aiming to deeply explore functional brain network features and classify them. For example, Song et al. [39] considered the spatial relationships of EEG and proposed a GCNN model for emotion recognition tasks, achieving relatively high accuracy in experiments. Additionally, Zhang et al. [40] proposed an MGCN-GAN model, using multi-layer GCNs to build generative adversarial networks, successfully explaining the complex nonlinear relationship between brain structure and functional connections, and achieving good classification performance on the Human Connectome Project (HCP) dataset. Huo et al. [41] considered temporal information and proposed a motion imagery classification model combining BiLSTM and GCN. By comprehensively considering both temporal and spatial information and using GCN for feature extraction and classification, they achieved an average accuracy of 94.64% on the PhysioNet dataset. Furthermore, Wang et al. [42] proposed a PGCNN model, utilizing Phase Locking Value (PLV) to construct functional connectivity matrices and employing shallow GCN models for emotion classification. The above literature demonstrates the feasibility of using brain functional connectivity combined with GCNs for EEG signal classification. Although the topological relationships between electrodes have been considered, the functional connections between them are often overlooked. Moreover, there is little research analyzing the differences in functional connectivity between real motor tasks and motor imagery tasks. Given that the perception and execution of movements require coordinated cooperation among various brain regions, especially in the context of motor imagery classification based on deep learning models, it is essential to fully consider the topological relationships between electrodes across the entire brain and their functional connections.

In summary, the integration of brain functional connectivity analysis with GCN models addresses the issue of overlooking inherent relationships between different electrodes in convolutional neural networks. As electrode positions and functional connections do not necessarily correspond, brain network analysis enables exploration of the working mechanisms and intrinsic connections between brain regions. Therefore, this study combines brain network analysis with GCN while fully considering the topological relationships between electrode positions to achieve classification recognition of motor imagery features and real movement features on the PhysioNet public dataset. Experimental results demonstrate that the algorithm proposed in this study outperforms other methods for identifying motor imagery EEG signals.

III. Materials and Methods

To achieve the recognition of the EEG signals of real movement and motor imagery tasks, and to analyze the difference in brain functional connectivity between the two, this paper proposes a method of motor behavior recognition by combining brain functional connectivity and graph neural network, and its technical route is shown in Fig.1.

A. Brain Functional Connectivity Measurements

Multiple different functional connectivity metrics were employed to comprehensively understand the connectivity relationship between various brain regions during the process of perception and motor execution. These include coherence and phase synchronization-based metrics, among which Phase-Locking Value [43] (PLV) and Phase Lag Index [44] (PLI) are utilized as phase synchronization-based metrics. These metrics assess the phase relationship between two electrodes, analyzing functional connectivity within the brain using phase synchronization methods. For coherence-based metrics, Spectral coherence [45] (COH) and Phase Slope Index [46] (PSI) were employed. Spectral coherence measures the linear relationship between two signals within a specific frequency band, while phase slope index quantifies the directional coupling between two signals. By integrating coherence-based and phase synchronization-based metrics, this analysis aims to provide a more comprehensive understanding of the functional

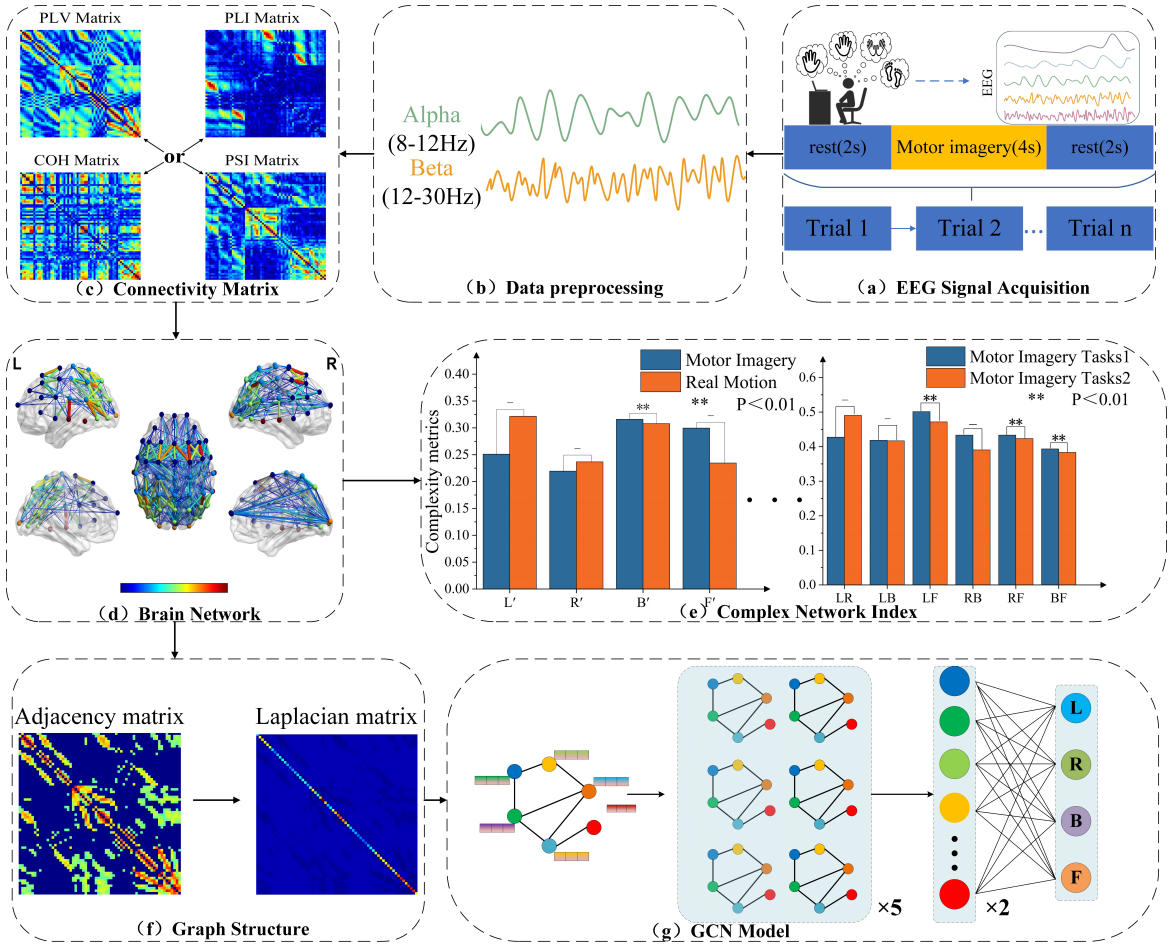

Fig. 1. Technology Roadmap. (a): Real and motor imagery EEG signals from subjects were acquired using a 64-lead device with a sampling rate of 160 Hz. (b): Preprocessing of EEG signals, including filtering, removal of ocular and other artifacts, etc. (c): Calculation of PLV, PLI, COH, and PSI brain functional connectivity matrices for EEG signals. (d): Mapping brain networks after thresholding the brain functional connectivity matrix. (e): Computation of complex network metrics between different motion imagery tasks and between real motion and motion imagery for the same task. (f): Constructing Graph Structures Using Thresholded Brain Functional Connectivity Matrices. (g): The raw EEG signals and adjacency matrices were inputted into the designed GCN model containing five-layer graph convolution, five-layer graph pooling, and two-layer graph convolution, and the spatiotemporal features of the EEG signals were extracted and subjected to four classifications (L, R, B, F)

connectivity patterns between different brain regions during the perception and execution of movements.

1) Phase Locking Value: The Phase-Locking Value measures the phase difference between two channel signals. Assuming the electrodes X and Y their corresponding EEG signals are represented by $X(t)$ and $Y(t)$, and the phase difference between $X(t)$ and $Y(t)$ is denoted as $\theta(t)$, the definition of PLV is as follows:

$$PLV = \frac{1}{N}\left|\sum_{n=1}^{N} e^{j(\theta(t_n))}\right|, \tag{1}$$

Where N is the length of the signal $\theta(t)$, the values of the PLV matrix range from 0 to 1. Specifically, this range signifies complete independence (0) to perfect synchronization (1) between the two signals.

2) Phase Lag Index: Phase Lag Index and PLV are similar and can be used to measure the synchronization level between two channel signals. Their definition is as follows:

$$PLI = \left|\frac{1}{N}\sum_{n=1}^{N} sign(\theta(t_n))\right|, \tag{2}$$

Where $sign$ is utilized to denote the sign of the phase difference, indicating whether the phase difference is positive or negative.

3) Spectral coherence: Spectral coherence quantifies the correlation between signals $X(t)$ and $Y(t)$ in the frequency domain. To begin, utilize frequency domain transformation techniques, including Fourier transform and wavelet transform, to convert time-frequency signals into the frequency domain. Subsequently, estimate the power spectral densities $P_{xx}(f)$ and $P_{yy}(f)$, as well as the cross-power spectral density $P_{xy}(f)$, for each frequency f . With this information, compute the coherent function $K_{xy}(f)$ and spectral coherence value using the following two formulas.

$$K_{xy}(f) = \frac{P_{xy}(f)}{\sqrt{P_{xx}(f)P_{yy}(f)}}, \tag{3}$$

$$COH_{xy}(f) = |K_{xy}(f)|^2, \tag{4}$$

4) Phase slope index: Phase Slope Index is a metric used to assess the causal relationship between signals. Its core concept is that if the propagation speeds of waves at different

frequencies are similar, the phase difference between the signal source and the receiver will increase with the frequency. This increase is manifested as a positive slope in the phase spectrum. The definition of PSI is as follows:

$$PSI = \frac{\xi\left(\sum_{f\in F} K_{xy}(f)K_{xy}(f+\partial F)\right)}{std\left[\xi\left(\sum_{f\in F} K_{xy}(f)K_{xy}(f+\partial F)\right)\right]}, \quad (5)$$

B. Brain network analysis

The process of brain network analysis is outlined in detail in Fig. 2. Initially, for preprocessed EEG signals related to real motor execution and motor imagery tasks, brain functional connectivity matrices are computed using various functional connectivity metrics. Subsequently, these matrices undergo a thresholding process. Finally, distinct measures of complexity are computed to analyze the differences in brain networks between real motor execution and motor imagery tasks.

The complexity metrics used in the experiments include clustering coefficient, global efficiency, transferability, modularity, median centrality, congruence, and feature path length. These complexity metrics are defined as follows:

The clustering coefficient is employed to depict the closeness of nodes and their neighboring nodes within a network. The clustering coefficient of a node i (denoted as C_i) and the overall clustering coefficient of the entire network (denoted as CC)—that is, the average clustering coefficient across all nodes in the network—are defined as follows:

$$C_i = \frac{2l_i}{k_i(k_i-1)}, \quad (6)$$

$$CC = \frac{1}{N}\sum_{i=1}^{N} C_i, \quad (7)$$

Where k_i represents the number of neighboring nodes of node i, l_i denotes the actual number of edges among the k_i neighboring nodes of node i, and N is the total number of nodes in the network.

Global efficiency is the average reciprocal of the shortest path lengths l_{ij} between all pairs of nodes, providing a measure of the network's capacity for parallel information processing. It is defined as follows:

$$Ge = \frac{1}{N(N-1)}\sum_{i,j\in V, i\neq j}\frac{1}{l_{ij}}, \quad (8)$$

Transitivity refers to the property that if there is an edge between node i and node j, and there is also an edge between node i and node k, then there must be an edge between node j and node k. The definition of transitivity is as follows:

$$TRA = \frac{\sum_{i\in N} 2R_i}{\sum_{i\in N} D_i(D_i-1)}, \quad (9)$$

Where R_i represents the geometric mean of the number of triangles around the node i, and D_i represents the degree of node i.

Modularity measures the strength of a network's division into different subnetworks, with higher values indicating stronger connections among similar nodes and vice versa. Modularity is defined as:

$$MOD = \frac{1}{2e}\sum_{ij}\left[w_{ij} - \frac{D_iD_j}{2e}\right]\delta(c_i,c_j), \quad (10)$$

Where e represents the total number of edges in the network, w_{ij} denotes the connectivity between two nodes, and the function $\delta(c_i,c_j)$ is defined as 1 when nodes i j belong to the same community and 0 otherwise.

The betweenness centrality of a node represents the number of shortest paths in the network that include that node. It is defined as:

$$BC = \frac{1}{(N-1)(N-2)}\sum_{\substack{i,j,k\in N\\ i\neq j\neq k}}\frac{q_{kj}(i)}{q_{kj}}, \quad (11)$$

Where q_{kj} represents the sum of the shortest path counts between node k and node j, and q_{kj} represents the shortest path count between node k and node j that passes through node i.

If nodes with similar weights are connected in the network, the network is considered assortative. The assortativity coefficient is used to describe the level of connectivity between nodes with higher weights. It is defined as:

$$ASS = \frac{l^{-1}\sum_{(i,j)\in L_{ij}^w} D_iD_j - \left[l^{-1}\sum_{(i,j)\in L_{ij}^w}(D_i+D_j)/2\right]^2}{l^{-1}\sum_{(i,j)\in L_{ij}^w}\left(D_i^2+D_j^2\right)/2 - \left[l^{-1}\sum_{(i,j)\in L_{ij}^w}(D_i+D_j)/2\right]^2}, \quad (12)$$

The characteristic path length is the average of the shortest paths between any two nodes in a complex network. It reflects the level of connectivity among network nodes and is an important metric for measuring network information transmission efficiency. A shorter characteristic path length indicates better network connectivity. It is defined as:

$$SPL = \frac{1}{N(N-1)}\sum_{i,j\in N, i\neq j} l_{ij}, \quad (13)$$

C. GCN model design

We applied Phase Locking Value, Phase Lag Index, Spectral coherence, and Phase Slope Index to the brain signals in the alpha and beta frequency bands, considering the spatial characteristics of the EEG signals. Subsequently, we employed a Graph Convolutional Network model for decoding, followed by classification using a Softmax layer on the features extracted by GCN. The brain functional connectivity-based GCN model is illustrated in Fig. 3, and the model details are presented in Table I.

The designed GCN model for this study comprises five graph convolutional layers, five graph pooling layers, and two fully connected layers. To mitigate overfitting, L2 regularization, and batch normalization are incorporated. Additionally, a 50% dropout is applied to the graph convolutional layers. The Rectified Linear Unit (ReLU) function serves as the activation function to address the vanishing gradient problem. Finally, the Adam optimizer is employed for training with a learning rate of 0.001.

In the GCN model, the graph is defined as $G = (V, E, A)$, where V is the set of vertices (comprising 64 electrode

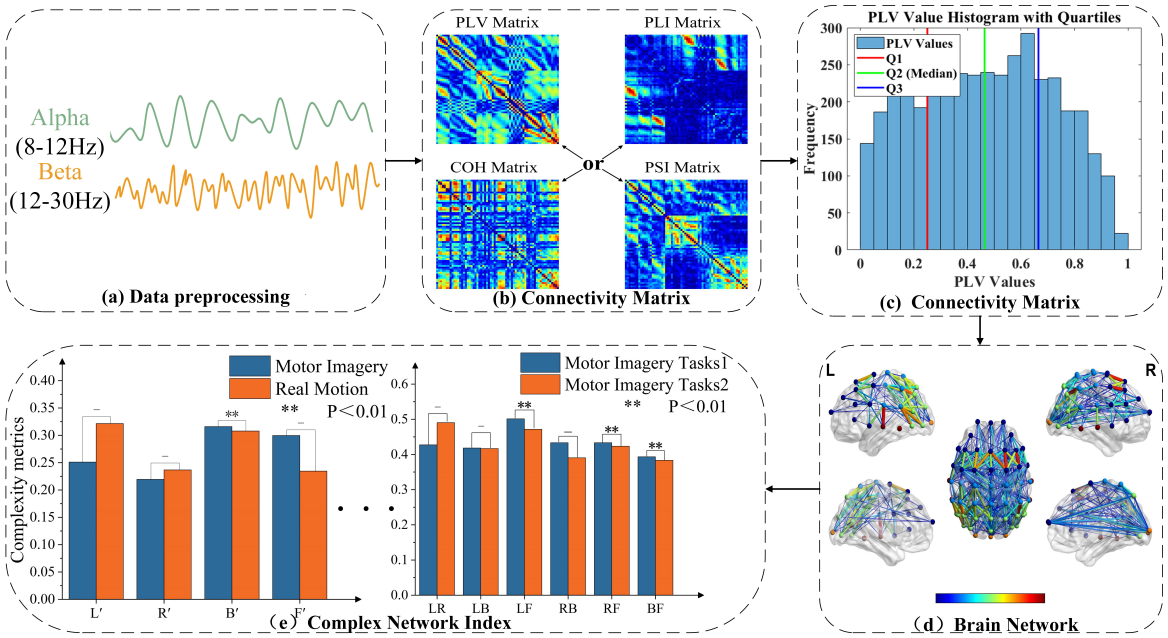

Fig. 2. Process of brain network analysis. (a): Preprocessing of EEG signals, including filtering, removal of ocular and other artifacts, etc. (b): Calculation of PLV, PLI, COH, and PSI brain functional connectivity matrices for EEG signals. (c): The connection weights in the brain functional connectivity matrix were formed into a vector of weights, using the upper quartile as the final threshold value. (d): Mapping brain networks after thresholding the brain functional connectivity matrix. (e): Computation of complex network metrics between different motion imagery tasks and between real motion and motion imagery for the same task.

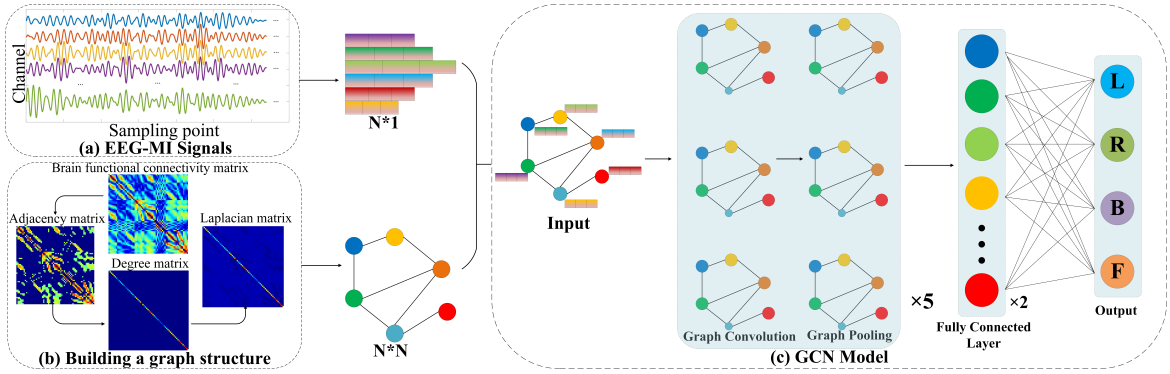

Fig. 3. GCN model design. (a): Preprocessed EEG signals. (b): Constructing graph structures through brain functional connectivity matrices, including adjacency, degree, and Laplacian matrixes. (c): The GCN model consists of a five-layer graph convolution layer, a five-layer graph pooling layer, two fully connected layers, and a softmax output layer.

TABLE I
GCN MODEL DETAILS

Layer	Filter	K-order	Pooling	Activation function
Input	-	-	-	-
Graphconv1	16	4	-	ReLU
Graphpooling1	16	-	2	-
Graphconv2	32	4	-	ReLU
Graphpooling2	32	-	2	-
Graphconv3	64	4	-	ReLU
Graphpooling3	64	-	2	-
Graphconv4	128	4	-	ReLU
Graphpooling4	128	-	2	-
Graphconv5	256	4	-	ReLU
Graphpooling5	256	-	2	-
FC1	512	-	-	ReLU
FC2	256	-	-	ReLU
Softmx	4	-	-	softmax

channels), E is the set of edges, and A represents the weighted adjacency matrix between two nodes as defined by the following formula:

$$A = \begin{cases} FC & \lambda \geq \theta \\ 0 & ' \lambda < \theta \end{cases}, \tag{14}$$

Where FC represents the brain functional connectivity matrix, and λ denotes the values within FC. When λ is greater than the threshold θ, it is considered a strong connection, and the original value is retained. If λ is less than the threshold θ, it is considered a weak connection, and the value is set to 0.

In the GCN model, graph convolution is achieved through graph Fourier transform. The Laplacian matrix of the graph is denoted as $L = D - A$, where D represents the degree matrix, with $D(i,i) = \sum_{j=1}^{n} A(i,j)$.

The definition of symmetrically normalized Laplacian ma-

trix is as follows:

$$L = I - D^{-\frac{1}{2}} A D^{-\frac{1}{2}}, \tag{15}$$

where I is the unit matrix.

Assuming the brain's electrical signal X, its graph fourier transform can be represented as:

$$\hat{X} = U^T X, \tag{16}$$

where U is an orthogonal matrix obtained through the singular value decomposition of the Laplacian matrix L. The specific process is as follows:

$$L = U \Lambda U^T, \tag{17}$$

where $U = [u_1, u_2, u_3, \cdots, u_N] \in R^{N*N}$ is the diagonal matrix containing the eigenvalues, $\Lambda = diag([\lambda_1, \lambda_2, \cdots \lambda_N])$ and is a diagonal matrix containing the eigenvalues.

The convolution of the signal X on the graph is defined as:

$$X * G = U((U^T G) \odot (U^T X)), \tag{18}$$

Where $\odot$ represents the Hadamard product.

Assuming the filter g_θ, the process of filtering signal X with $g_\theta(L)$ can be represented as:

$$Y = g_\theta(L)X = g_\theta(U \Lambda U^T)X = U g_\theta(\Lambda) U^T X, \tag{19}$$

However, due to the difficulty in directly computing $g_\theta(\Lambda)$, the calculation is performed using K–order Chebyshev polynomials:

$$g_\theta(\Lambda) = \sum_{k}^{k-1} \theta_k T_k(\tilde{\Lambda}), \tag{20}$$

Where θ_k represents the coefficients of the Chebyshev polynomial, $\tilde{\Lambda} = \frac{2\Lambda}{\lambda_{\max}} - I$

$$T_k\left(\tilde{\Lambda}\right) = \begin{cases} 1, k = 0 \\ \tilde{\Lambda}, k = 1 \\ 2\tilde{\Lambda} T_{k-1}(\tilde{\Lambda}) - T_{k-2}(\tilde{\Lambda}), k \geq 2 \end{cases}, \tag{21}$$

Therefore, the graph convolution operation can be reformulated as:

$$Y = U \sum_{k}^{k-1} \theta_k T_k(\tilde{\Lambda}) U^T X = \sum_{k}^{k-1} \theta_k T_k(\tilde{L}) X, \tag{22}$$

IV. Analysis of Experimental Results

This section begins with an introduction to the dataset and its preprocessing. Following this, we conduct a statistical and connectivity analysis of brain networks formed by various indicators of brain functional connections. The GCN model is then employed to classify the spatiotemporal features of EEG signals, followed by a detailed analysis of the experimental results.

A. Introduction to the data set

This study utilizes the publicly available PhysioNet dataset [47], the GigaDB publicly available dataset [48], and the motor imagery dataset of acute stroke patients from Xuanwu Hospital, Capital Medical University [49], to identify motor imagery tasks and evaluate the effectiveness and robustness of the proposed methods.

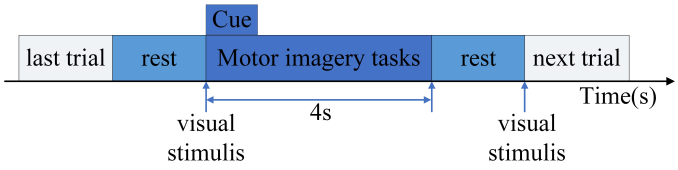

Fig. 4. Experimental Paradigms. The subject is cued to execute the real execution or MI task for four seconds while the cue appears, then rest until the next trial starts.

1) The PhysioNet Dataset: The PhysioNet public dataset was collected using a 64-channel device and includes EEG signals of real and imagined movements from 109 subjects (S1-S109), with a sampling rate of 160 Hz. Throughout the experimental process, participants engaged in 14 trials, consisting of 2 baseline segments and 3 experimental segments (each containing 4 tasks). The experimental paradigm, illustrated in Fig. 4, involved real and imagined movements of the left fist, right fist, both fists, and both feet. The specific tasks were as follows:

Task 1: The task objective appeared on the left or right side of the screen, and participants clenched and unclenched the corresponding fist until the target disappeared, followed by a rest period.

Task 2: Similar to Task 1, participants were instructed to imagine clenching and unclenching the corresponding fist until the target disappeared, followed by a rest period.

Task 3: The task objective appeared at the top or bottom of the screen, and participants clenched and unclenched both fists (top) or both feet (bottom) until the target disappeared, followed by a rest period.

Task 4: Similar to Task 3, participants were instructed to imagine clenching and unclenching both fists (top) or both feet (bottom) until the target disappeared, followed by a rest period.

In this study, to enhance computational efficiency, only 30 participants (S1-S30) were utilized for experimentation.

2) The GigaDB Dataset: This dataset was collected using a 64-channel device and includes EEG signals of real and imagined movements from 52 subjects (S1-S52), with a sampling rate of 512 Hz. The dataset comprises two tasks: actual movement or motor imagery of the left hand and right hand, each lasting three seconds. In this study, only 20 subjects (S1-S20) were used to test the proposed methods. For more details about this dataset, please refer to reference [48].

3) The Xuanwu Hospital Dataset: This dataset was collected using the international 10-10 electrode placement system (including 29 EEG electrodes and two EOG electrodes) from 50 acute stroke patients, with a sampling rate of 500 Hz. During the experiments, patients performed 40 trials, each lasting 8 seconds (2 seconds for the instruction phase, 4 seconds for the motor imagery task, and 2 seconds for the rest phase). Each trial included two motor imagery tasks. In the experimental phase, patients were asked to imagine gripping a spherical object with their left or right hand. In this study, only 5 subjects (S1-S5) were used to test the proposed methods. For more details about this dataset, please refer to reference [49].

B. Data preprocessing and environment configuration

The preprocessing of the aforementioned open datasets follows a procedure similar to other EEG signal processing workflows. While aiming to retain the original information as much as possible, early-stage data processing involved the removal of ocular artifacts and other artifacts to ensure the acquisition of high-quality data. Subsequently, a fourth-order zero-phase Butterworth bandpass filter was applied to capture EEG frequency bands most relevant to motor rhythms [50], primarily including alpha waves (8-12Hz) and beta waves (13-30Hz). This preprocessing was consistently applied to all three public datasets used in the study. The preprocessing of EEG data in this study was conducted using EEGLAB and Python toolkits, while the GCN model was implemented using the TensorFlow framework. Given the inclusion of 109 subjects in the PhysioNet open dataset, this study opted to enhance computational efficiency by selecting the first 30 subjects for experimentation. The preprocessed data from these 30 subjects were then split into training and validation sets in a 9:1 ratio. The same approach for splitting the data into training and validation sets was applied to the other two datasets as well. All training and testing of neural network models were carried out on a server equipped with an Nvidia 4090 GPU.

C. Statistical analysis based on functional brain connectivity indicators

To validate distinctions between motor imagery and actual movement, as well as among different motor imagery tasks, brain functional connectivity metrics based on coherence and phase synchronization were utilized to compute networks in the alpha and beta frequency bands. However, due to the faint amplitude of EEG signals and the prevalence of numerous weak connections, which may be attributed to noise, these weak connections cannot accurately represent interregional connections. Therefore, appropriate thresholds were selected to construct functional brain networks. For this purpose, connection weight values from the brain functional connectivity matrices for the two frequency bands were compiled into a weight vector, with the upper quartile serving as the final threshold.As shown in Fig. 5, the frequency histogram of the weight vector of the PLV matrix is displayed.Finally, common network characteristic parameters in complex networks were utilized to conduct paired t-tests for significant differences in the thresholded brain networks across different frequency bands, as presented in Tables II to IX.

The results of the significant difference analysis in Tables II to IX indicate that there are significant differences in the alpha and beta bands among LF, RF, and BF during different motor imagery tasks. When comparing actual movement with motor imagery during the same task, brain functional networks based on phase synchronization (PLV and PLI) exhibit significantly stronger differences than those based on coherence indices (PSI and COH), and the significant differences are primarily concentrated in the R/ region. Given that the alpha and beta bands are the two most relevant bands to motor imagery, the results of the significance analysis for the alpha and beta bands are essentially similar.

TABLE II
SIGNIFICANT DIFFERENCES IN TWO-BAND PLV NETWORKS BETWEEN DIFFERENT MOTOR IMAGERY TASKS

Frequency	α						β					
Groups	LR	LB	LF	RB	RF	BF	LR	LB	LF	RB	RF	BF
CC	-	-	**	-	**	**	-	-	**	-	**	**
Ge	-	-	**	-	**	**	-	-	**	-	**	**
TRA	-	-	**	-	**	**	-	-	**	-	**	**
MOD	-	-	**	-	**	**	-	-	**	-	**	**
BC	-	-	**	-	**	**	-	-	-	-	-	-
ASS	-	-	-	-	-	-	-	-	-	-	*	*
SPL	-	-	**	-	**	**	-	-	**	-	**	**

LR: left fist vs. right fist. LB: left fist vs. both fists. LF: left fist vs. both feet. RB: right fist vs. both fists. RF: right fist vs. both feet. BF: both fists vs. both feet.
-: indicates no significant difference.
*: Means $p < 0.05$. **: Means $p < 0.001$.

TABLE III
SIGNIFICANT DIFFERENCES IN TWO-BAND PLI NETWORKS BETWEEN DIFFERENT MOTOR IMAGERY TASKS

Frequency	α						β					
Groups	LR	LB	LF	RB	RF	BF	LR	LB	LF	RB	RF	BF
CC	-	-	**	-	**	**	-	-	**	-	**	**
Ge	-	-	**	-	**	**	-	-	**	-	**	**
TRA	-	-	**	-	**	**	-	-	**	-	**	**
MOD	-	-	**	-	**	**	-	-	**	-	**	**
BC	-	-	**	-	**	**	-	-	**	-	**	**
ASS	-	-	-	-	-	-	-	-	**	-	*	*
SPL	-	-	**	-	**	**	-	-	**	-	**	**

LR: left fist vs. right fist. LB: left fist vs. both fists. LF: left fist vs. both feet. RB: right fist vs. both fists. RF: right fist vs. both feet. BF: both fists vs. both feet.
-: indicates no significant difference.
*: Means $p < 0.05$. **: Means $p < 0.001$.

TABLE IV
SIGNIFICANT DIFFERENCES IN TWO-BAND COH NETWORKS BETWEEN DIFFERENT MOTOR IMAGERY TASKS

Frequency	α						β					
Groups	LR	LB	LF	RB	RF	BF	LR	LB	LF	RB	RF	BF
CC	-	-	**	-	**	**	-	-	**	-	**	**
Ge	-	-	**	-	**	**	-	-	**	-	**	**
TRA	-	-	**	-	**	**	-	-	**	-	**	**
MOD	-	-	-	-	-	-	-	-	**	-	**	**
BC	-	-	**	-	**	**	-	-	**	-	**	**
ASS	-	-	-	-	-	-	*	-	-	-	-	-
SPL	-	-	**	-	**	**	-	-	**	-	**	**

LR: left fist vs. right fist. LB: left fist vs. both fists. LF: left fist vs. both feet. RB: right fist vs. both fists. RF: right fist vs. both feet. BF: both fists vs. both feet.
-: indicates no significant difference.
*: Means $p < 0.05$. **: Means $p < 0.001$.

TABLE V
SIGNIFICANT DIFFERENCES IN TWO-BAND PSI NETWORKS BETWEEN DIFFERENT MOTOR IMAGERY TASKS

Frequency	α						β					
Groups	LR	LB	LF	RB	RF	BF	LR	LB	LF	RB	RF	BF
CC	-	-	**	-	**	**	-	-	-	-	*	*
Ge	-	-	**	-	**	**	-	-	**	-	**	**
TRA	-	-	**	-	**	**	-	-	-	-	*	*
MOD	-	-	-	-	-	-	-	-	**	-	**	**
BC	-	-	**	-	**	**	-	-	**	-	**	**
ASS	-	-	-	-	-	-	-	-	-	-	-	-
SPL	-	-	**	-	**	**	-	-	**	-	**	**

LR: left fist vs. right fist. LB: left fist vs. both fists. LF: left fist vs. both feet. RB: right fist vs. both fists. RF: right fist vs. both feet. BF: both fists vs. both feet.
-: indicates no significant difference.
*: Means $p < 0.05$. **: Means $p < 0.001$.

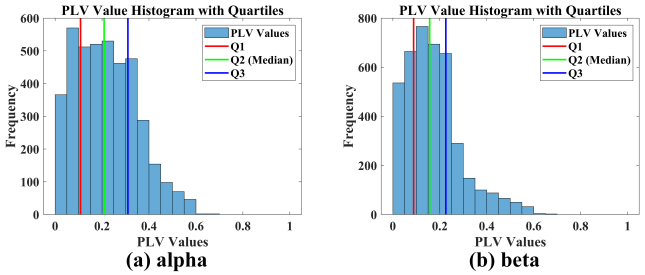

Fig. 5. Frequency histograms of the PLV brain networks corresponding to alpha and beta bands.

TABLE VI
SIGNIFICANT DIFFERENCES IN TWO-BAND PLV NETWORKS BETWEEN MOTION IMAGERY AND REAL MOTION

Frequency	α				β			
Groups	L/	R/	B/	F/	L/	R/	B/	F/
CC	-	-	**	-	-	*	**	-
Ge	-	-	**	-	-	*	**	-
TRA	-	-	**	-	-	*	**	-
MOD	-	-	-	-	-	-	-	-
BC	-	*	-	-	-	-	-	-
ASS	-	-	-	-	-	-	-	-
SPL	*	-	**	-	-	-	**	-

L/: Motor Imagery of the left fist vs. Real Movement of the left fist.
R/: Motor Imagery of the right fist vs. Real Movement of the right fist.
B/: Motor Imagery of the both fists vs. Real Movement of the both fists.
F/: Motor Imagery of the both feet vs. Real Movement of the both feet.
-: indicates no significant difference.
*: Means $p < 0.05$. **: Means $p < 0.001$.

D. Brain network analysis based on functional brain connectivity metrics

Following a significant analysis of four brain networks in the alpha and beta frequency bands, notable differences were observed among different motor imagery tasks, particularly between upper and lower limb tasks. The significance disparity between motor imagery and actual motor execution was most pronounced during bimanual fist tasks, with the greatest distinctions apparent in brain functional connectivity indices based on phase synchronization metrics. Consequently, the BrainNet Viewer toolbox [51] was utilized to illustrate the PLV, PLI, COH, and PSI network topologies for the four motor imagery tasks. Additionally, the PLV and PLI network topologies during bimanual fist motor imagery and actual motor execution were depicted.

TABLE VII
SIGNIFICANT DIFFERENCES IN TWO-BAND PLI NETWORKS BETWEEN MOTION IMAGERY AND REAL MOTION

Frequency	α				β			
Groups	L/	R/	B/	F/	L/	R/	B/	F/
CC	-	-	**	-	-	-	*	-
Ge	*	-	**	-	-	-	*	-
TRA	-	-	**	-	-	-	*	-
MOD	-	-	-	-	-	-	-	-
BC	-	-	-	-	-	-	-	-
ASS	-	-	-	-	-	-	-	-
SPL	-	*	**	-	-	-	**	-

L/: Motor Imagery of the left fist vs. Real Movement of the left fist.
R/: Motor Imagery of the right fist vs. Real Movement of the right fist.
B/: Motor Imagery of the both fists vs. Real Movement of the both fists.
F/: Motor Imagery of the both feet vs. Real Movement of the both feet.
-: indicates no significant difference.
*: Means $p < 0.05$. **: Means $p < 0.001$.

TABLE VIII
SIGNIFICANT DIFFERENCE IN THE TWO-BAND COH NETWORK BETWEEN MOTOR IMAGERY AND REAL MOVEMENT

Frequency	α				β			
Groups	L/	R/	B/	F/	L/	R/	B/	F/
CC	-	-	-	-	-	-	-	-
Ge	-	-	-	-	-	-	-	-
TRA	-	-	-	-	-	-	-	-
MOD	-	-	-	-	-	**	*	*
BC	-	-	-	-	-	-	-	-
ASS	-	-	-	-	-	**	*	-
SPL	-	-	-	-	-	-	-	*

L/: Motor Imagery of the left fist vs. Real Movement of the left fist.
R/: Motor Imagery of the right fist vs. Real Movement of the right fist.
B/: Motor Imagery of the both fists vs. Real Movement of the both fists.
F/: Motor Imagery of the both feet vs. Real Movement of the both feet.
-: indicates no significant difference.
*: Means $p < 0.05$. **: Means $p < 0.001$.

TABLE IX
SIGNIFICANT DIFFERENCES IN TWO-BAND PSI NETWORKS BETWEEN MOTION IMAGERY AND REAL MOTION

Frequency	α				β			
Groups	L/	R/	B/	F/	L/	R/	B/	F/
CC	-	-	-	-	-	-	-	-
Ge	-	-	-	-	-	-	*	-
TRA	-	-	-	-	-	-	-	-
MOD	-	-	-	-	-	-	-	-
BC	-	-	*	-	-	-	-	-
ASS	-	-	-	-	-	*	*	-
SPL	-	-	-	-	-	-	-	*

L/: Motor Imagery of the left fist vs. Real Movement of the left fist.
R/: Motor Imagery of the right fist vs. Real Movement of the right fist.
B/: Motor Imagery of the both fists vs. Real Movement of the both fists.
F/: Motor Imagery of the both feet vs. Real Movement of the both feet.
-: indicates no significant difference.
*: Means $p < 0.05$. **: Means $p < 0.001$.

Fig. 6 to 9 presents the four brain networks and their corresponding topologies in the alpha and beta frequency bands during the execution of four motor imagery tasks. Different colors of nodes in the network topology represent different brain regions (specifically: blue - frontal lobe, light blue - central region, green - parietal lobe, orange - occipital lobe, and red - temporal lobe). The varying intensity and thickness of lines indicate the strength of connections in the brain network. Connectivity between brain regions increased during the four motor imagery tasks, particularly among the frontal lobe, parietal lobe, occipital lobe, and temporal lobe, as well as the primary motor cortex, premotor area, supplementary motor area, somatosensory cortex, and visual cortex. Notably, connectivity was stronger for hand-related tasks (left fist, right fist, and bimanual fists) compared to foot-related tasks, with bimanual fist connectivity being the most significant, especially in the PLV brain network. Fig. 10 reveals enhanced connectivity between frontal, parietal, occipital, and temporal lobes, as well as the primary motor cortex, premotor area, supplementary motor area, somatosensory cortex, and visual cortex during both bimanual fist motor imagery and actual tasks. Importantly, the connectivity during actual motor execution was found to be stronger than during motor imagery tasks.

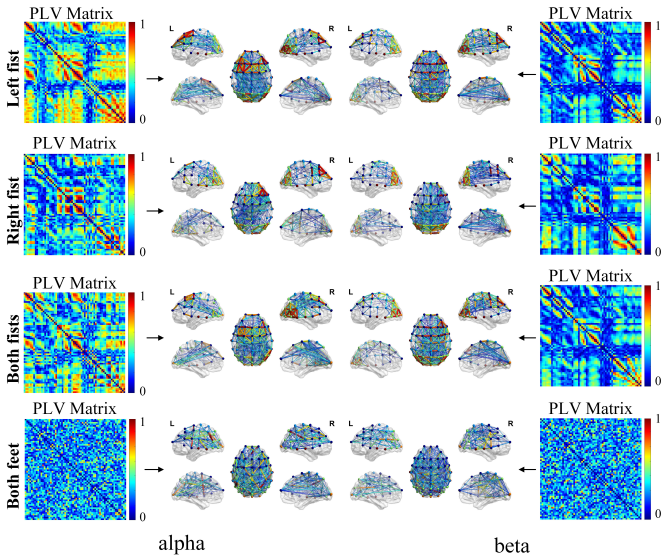

Fig. 6. Topology of the PLV brain network for motor imagery alpha and beta bands. Each row in the figure represents a different motor imagery task. The left half depicts the connectivity matrix of brain functions in the alpha band and the corresponding brain network structure after thresholding. The right half shows the connectivity matrix of brain functions in the beta band and the corresponding brain network structure after thresholding.

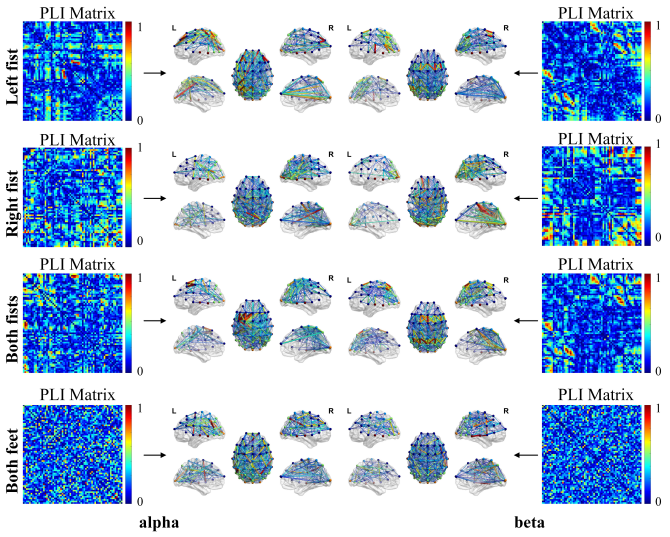

Fig. 7. Topology of the PLI brain network for motor imagery alpha and beta bands. Each row in the figure represents a different motor imagery task. The left half depicts the connectivity matrix of brain functions in the alpha band and the corresponding brain network structure after thresholding. The right half shows the connectivity matrix of brain functions in the beta band and the corresponding brain network structure after thresholding.

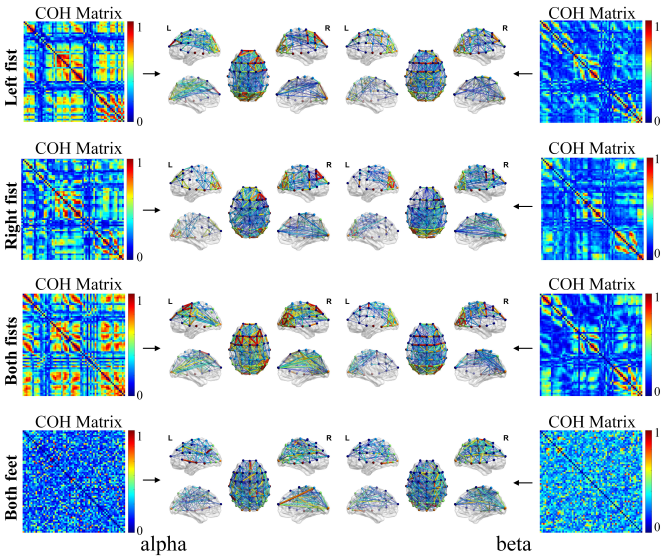

Fig. 8. Topology of the COH brain network for motor imagery alpha and beta bands. Each row in the figure represents a different motor imagery task. The left half depicts the connectivity matrix of brain functions in the alpha band and the corresponding brain network structure after thresholding. The right half shows the connectivity matrix of brain functions in the beta band and the corresponding brain network structure after thresholding.

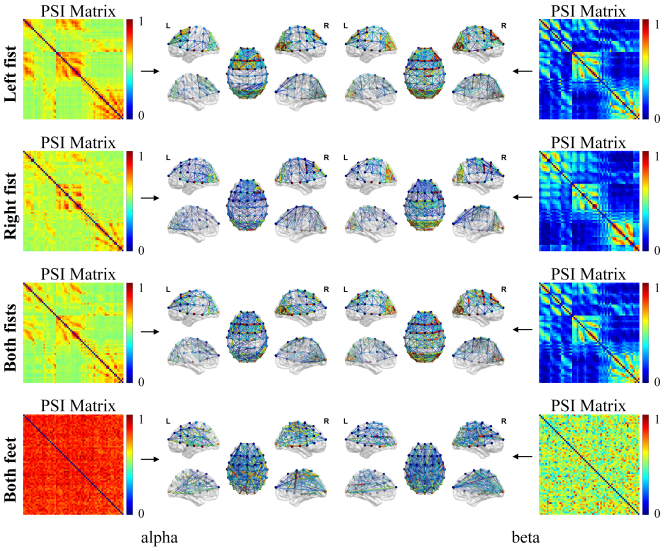

Fig. 9. Topology of the PSI brain network for motor imagery alpha and beta bands. Each row in the figure represents a different motor imagery task. The left half depicts the connectivity matrix of brain functions in the alpha band and the corresponding brain network structure after thresholding. The right half shows the connectivity matrix of brain functions in the beta band and the corresponding brain network structure after thresholding.

E. Classification of Spatio-temporal features

As indicated in Section IV-D, it is evident that the phase-locking value brain network exhibits more pronounced connectivity among the frontal, parietal, occipital, and temporal lobes, as well as the primary motor cortex, premotor area, supplementary motor area, somatosensory cortex, and visual cortex, compared to the other three brain networks. To further validate the impact of different functional brain networks on experimental results, different brain networks were computed using PLV, PLI, COH, and PSI, and corresponding graph structures were experimentally evaluated. As shown in Fig. 11, the brain network and graph structure constructed using PLV demonstrated significantly superior accuracy and lower loss on the training set compared to the other three functional connectivity indices. In the case of the L, B, R, and F motor imagery four-classification scenarios, the accuracy on the validation set

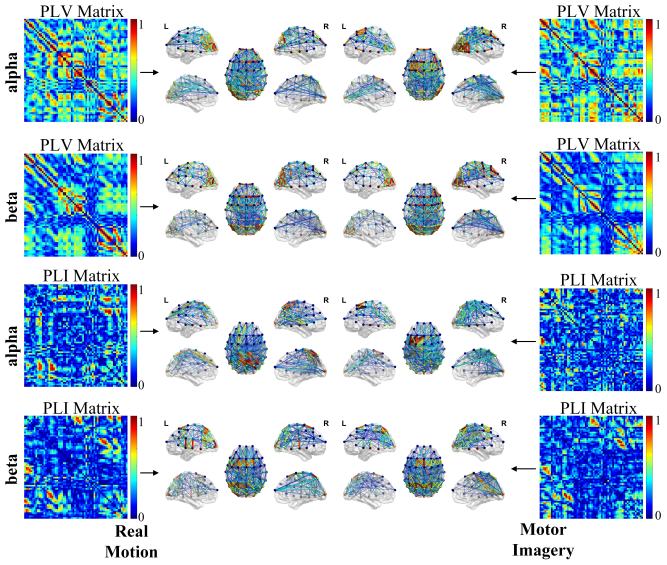

Fig. 10. PLV and PLI network topologies for two-fisted real motion and motion-imagined alpha and beta bands. Each row in the figure represents different frequency bands, including alpha and beta bands. The left half illustrates the PLV and PLI brain functional connectivity matrices, along with their corresponding brain network topology, during the real bimanual movement task. The right half shows the PLV and PLI brain functional connectivity matrices, and the corresponding brain network topology during the imagined bimanual movement task.

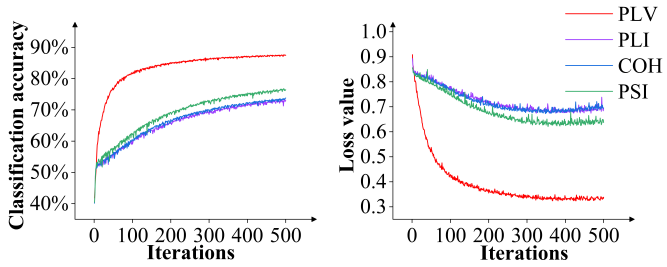

Fig. 11. Thirty participants were employed to assess accuracy and loss on four different brain network validation sets in a four-classification task.

reached 88.39%. Consequently, all subsequent experimental analyses employed the PLV functional connectivity index to construct the graph structure.

Due to the nonlinear nature and weak amplitude of EEG signals, we conducted experiments to validate whether our designed model could extract deep-level features from EEG signals. We designed GCN models with varying numbers of layers for experimental verification, and the implementation details of different frameworks are outlined in Table XI. As illustrated in Fig. 12 for different-layer GCN models, the classification accuracy improved with an increase in the number of graph convolution layers and graph pooling layers. However, after reaching five graph convolution layers and five graph pooling layers, the classification accuracy reached its peak and did not show further improvement. Moreover, the loss value was optimal compared to other layer configurations. Considering both the classification accuracy and loss on the validation set, the experimentally chosen structure of five graph convolution layers and five graph pooling layers was found to be capable of effectively extracting spatiotemporal features from EEG signals.

TABLE X
DETAILS OF THE IMPLEMENTATION OF THE DIFFERENT LAYERS OF THE FRAMEWORK

Framework	Number of conv Layers	Number of pooling layers	Number of filters
C-P-Fc1-Fc2	1	1	32
(C-P)*2-Fc1-Fc2	2	2	32/64
(C-P)*3-Fc1-Fc2	3	3	32/64/128
(C-P)*4-Fc1-Fc2	4	4	32/64/128/256
(C-P)*5-Fc1-Fc2	5	5	32/64/128/256/512
(C-P)*6-Fc1-Fc2	6	6	16/32/64/128/256/512

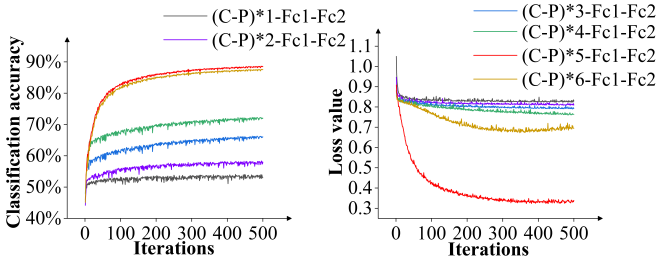

Fig. 12. In a four-classification task, a comparative experiment was conducted with 30 participants using GCN models with varying numbers of layers.

V. DISCUSSION

Through the experimental results in section IV, we have discovered that brain networks constructed using Phase Locking Value are more suitable for research in the classification of motor imagery. Additionally, the functional connectivity of the brain during actual movements is found to be stronger than that during imagined movements. Constructing PLV brain functional connectivity metrics for the alpha and beta frequency bands allows for a comprehensive consideration of the topological relationships between electrodes. The PLV metrics effectively capture the spatiotemporal characteristics of the EEG signals, facilitating the efficient decoding of EEG signals. The application of GCN models enables the extraction of spatiotemporal features from both the EEG signals and the brain functional connectivity matrix, thereby improving the classification performance of motor imagery brain-machine interfaces.

In Section IV-C, during the brain network analysis, we adopted the upper quartile as the final threshold. Here, we explain the rationale behind this choice through experimental analysis and discuss the potential impact of different thresholding strategies on the results. Specifically, we extracted the connection weights from the brain functional connectivity matrix into a weight vector and conducted comparative experiments using the upper quartile (Q3), median (Q2), lower quartile (Q1), and the original matrix without thresholding (Original). The experiments covered both multi-subject and single-subject results, with relevant data shown in the Table XI. The results indicate that choosing the upper quartile (Q3) as the threshold does not significantly differ in accuracy compared to other thresholding methods. In terms of time complexity, Q3 is slightly superior to the other three thresholding options. This

TABLE XI
POTENTIAL IMPACT OF DIFFERENT THRESHOLDING STRATEGIES ON THE RESULTS

Subject	Metrics	Threshold			
		Q1	Q2	Q3	Original
S11	Acc	99.03%	99.10%	99.17%	99.02%
	F1	99.03%	99.09%	99.16%	99.02%
	Time(s)	140	142	140	141
S29	Acc	97.98%	98.31%	98.52%	97.90%
	F1	97.97%	98.29%	98.51%	97.89%
	Time(s)	192	193	190	192
S1-S30	Acc	88.55%	88.47%	88.93%	88.50%
	F1	88.54%	88.46%	88.93%	88.49%
	Time(s)	143932	143136	137159	143600

advantage is particularly noticeable in multi-subject experiments, where using the upper quartile significantly reduces time complexity. Even in single-subject scenarios, Q3 still demonstrates some superiority. Therefore, selecting the upper quartile as the threshold not only ensures accuracy but also provides a clear advantage in terms of computational resource utilization. Additionally, this choice is also beneficial for visualizing brain networks. The upper quartile effectively removes weak connections with low weights, making the nodes and edges in the network graph clearer and more concise, highlighting key functional connections. This not only helps to present the core structure of the brain network more intuitively but also enhances the ability to identify important brain regions and functional modules, thus providing more valuable insights for further brain science research.

As shown in Tables II to V, significant differences among different motor imagery tasks are evident, primarily between upper and lower limbs (LF, RF, and BF). The analysis attributes this distinction to the fact that during upper limb motor imagery, neural regulation is mainly governed by the motor cortex in the brain. Signals are transmitted through the nerves to the spinal cord, eventually controlling the muscles responsible for upper limb movements. While a similar process occurs during lower limb motor imagery, neural signals need to traverse the spinal cord to control muscles below the waist. The motor cortex in the brain must control a greater number of neurons for lower limb movements, involving a more extensive network of neurons and a more complex neural circuit compared to upper limb movements [52]. Furthermore, no significant differences were observed in several brain network characteristic parameters between other task combinations (such as LR with LB and RB), indicating a similarity in the brain's functional connectivity structure between the left fist and right fist, left fist and both fists, as well as right fist and both fists. As indicated in Tables VI to IX, significant differences between actual movements and motor imagery for the same task suggest that these differences are mainly pronounced during tasks involving the right fist and both fists (R$\prime$ and B$\prime$). Moreover, the significance of differences based on phase synchronization-based brain functional connectivity metrics (PLV and PLI) tends to be slightly stronger than those based on coherence-based metrics (COH and PSI). The reason for this lies in the fact that coherence-based metrics are influenced by both the amplitude and phase of EEG signals when analyzing connectivity relationships. In contrast, phase synchronization-based metrics can effectively mitigate the impacts of EEG signal amplitude and phase, resulting in a more robust detection of significant differences.

As illustrated in Fig. 6 to 10, the four brain network topologies during motor imagery tasks reveal enhanced connectivity between different brain regions, particularly in the frontal, parietal, occipital, and temporal lobes, when performing upper limb motor imagery tasks (L, R, and B). These regions correspond to the primary motor cortex, pre-motor area, supplementary motor area, somatosensory cortex, and visual cortex in the cerebral cortex. In contrast, during lower limb motor imagery tasks (F), connectivity relationships are observed across the entire brain, validating the significant differences identified in our significance analysis between upper and lower limbs. The brain network during lower limb motor imagery suggests that, compared to upper limb motor imagery, a more widespread coordination of neural elements across the entire brain is required to control the execution of lower limb motor tasks. This outcome underscores the idea that the perception and execution of movement involve coordinated efforts from various brain regions throughout the entire brain, extending beyond regions solely dedicated to motor perception. Particularly in the context of motion imagery classification using deep learning models, it becomes crucial to consider the features of signals from all brain regions comprehensively.

For a deeper validation of the performance of our proposed model, we divided the data into 10 folds. One fold served as the validation set, while the remaining nine folds constituted the training set, employing ten-fold cross-validation. The results, depicted in Fig. 13, show that the highest accuracy reached 90.01%, the lowest accuracy was 87.03%, and the average accuracy was 88.35%. This provides further evidence of the stability and reliability of our proposed model. For further validation of the model's generalization performance, experimental verification was conducted on the GigaDB dataset, yielding a result of 84.61%. This also indicates that our proposed model performs well on different datasets and possesses strong generalization capabilities. Given that both datasets were collected using 64-channel devices, we considered the majority of motor imagery-based brain-computer interface research, which focuses primarily on healthy subjects, with relatively fewer studies involving patients with motor disorders. However, motor imagery technology is mainly applied in the treatment of patients with motor dysfunction. Therefore, to further validate the model's generalization capability and evaluate the applicability and effectiveness of motor imagery technology across different populations, we conducted validation on a motor imagery dataset collected from acute stroke patients using a 32-channel device. The experimental results, as shown in the Fig. 14, demonstrate that the highest accuracy for a single subject reached 93.55%, and in the multi-subject scenario, the accuracy reached 95.77%. These results indicate that our model performs excellently in different application scenarios and exhibits strong generalization capability.

To validate the performance and robustness of the proposed algorithm, we randomly selected ten subjects (S4, S9, S11,

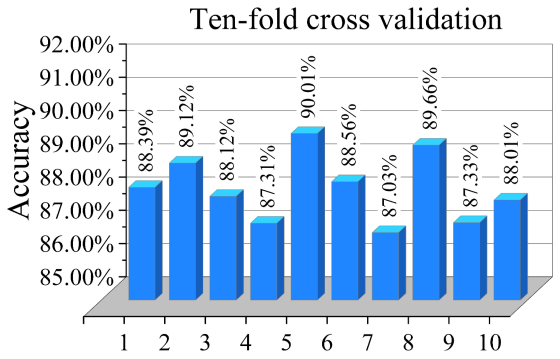

Fig. 13. After dividing the data into 10 parts, with one part used as the validation set and the remaining nine parts used as the training set, the results of ten-fold cross-validation are obtained.

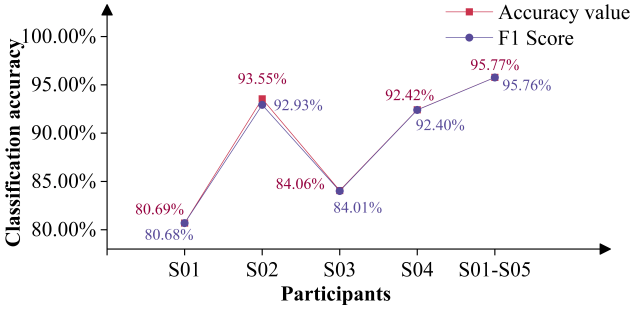

Fig. 14. Results of the model in single-subject and multi-subject experiments on a motor imagery dataset of acute stroke patients collected using a 32-channel device.

S17, S20, S22, S25, S29, S30, and S32) from the PhysioNet public dataset for individual subject analysis. The experimental results are depicted in Fig. 15. The results demonstrate that under single-subject analysis, the highest accuracy reached 99.83%, the lowest accuracy was 98.80%, and the average accuracy was 99.33%. The highest F1 score reached 99.80%, the lowest F1 score was 98.79%, and the average F1 score reached 99.31%. As the designed model in this study extracts spatiotemporal features from EEG signals, taking into account the topological relationships between electrodes, it reduces the complexity of EEG signals. Consequently, the model achieves commendable results across different subjects. This outcome also indicates that the model is capable of addressing inter-individual differences, making it more suitable for individualized applications.

As shown in Table XII, to further verify the performance of the proposed model, we compared it with several advanced motor imagery classification algorithms, including HR-SNN [53], MAML-CNN [54], RACNN [55], Mi-BMInet [56], and 3DCNN-LSTM [57]. These studies all used the publicly available PhysioNet dataset. The results demonstrate that our method exhibits superior classification performance compared to other methods, achieving an accuracy of 88.39%. This affirms that the integration of brain functional connectivity

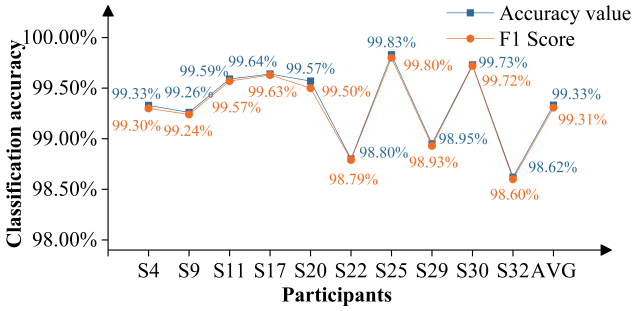

Fig. 15. Individual analyses were performed, presenting the accuracy and F1 scores of ten participants (S4, S9, S11, S17, S20, S22, S25, S29, S30, and S32), along with their respective average values.

TABLE XII
COMPARISON RESULTS OF DIFFERENT METHODS

Methods	Number of channels	Number of subjects	Maximum accuracy
HR-SNN	64	105	74.95%
MAML-CNN	17	104	80.6%
RACNN	14	104	76.9%
Mi-BMInet	64	105	82.99%
3DCNN-LSTM	64	20	86.13%
This work	64	30	88.39%

metrics with Graph Convolutional Networks is advantageous for extracting spatiotemporal features from EEG signals and decoding brain electrical activity. There are three main reasons for the success of our approach: (1) Building a brain functional connectivity network for the complex/dynamic system of the brain helps preserve crucial information about time and space scales. (2) Leveraging the success of deep learning in fields such as computer vision, constructing a graph structure using brain functional connectivity metrics, and employing GCN for classification allows for the consideration of both local and global information between each electrode. This approach captures complex relationships among electrodes and contextual information in EEG signals, contributing to improved classification performance. (3) The integration of brain functional connectivity with GCN enables the extraction of deep-level features from EEG signals, enhancing the model's ability to discern patterns and nuances in brain activity.

VI. CONCLUSION

Through the analysis of brain EEG signals during both imagined and actual movements, a 4-classification model for motor imagery tasks is proposed, incorporating brain networks and Graph Convolutional Networks based on various brain functional connectivity indices. Four types of brain functional connections, namely Phase Locking Value, Phase Lag Index, Spectral coherence, and Phase Slope Index are employed to construct brain networks for different motor imagery tasks as well as real movement tasks. Significance analysis is conducted using T-tests. Graph structures are built using brain functional connections, and the GCN model is utilized to extract spatiotemporal features and deeper abstract features from EEG signals for the classification of motor imagery tasks. The model achieves an accuracy of 88.39% in the multi-subject

group, with individual subject groups achieving classification accuracies above 98.62%. The highest accuracy reaches 99.83%, demonstrating significant advantages compared to other traditional and deep learning algorithms. The research results not only confirm the effectiveness of combining brain functional connections and GCN models for recognizing motor imagery features but also expand the methods for analyzing motor imagery features. This provides new perspectives for representing and recognizing EEG signal features, with implications for research in EEG-based classification tasks. The combination of brain functional connections and GCN models not only has practical value for motor imagery feature recognition but also contributes to the exploration of EEG signal features, offering valuable insights for classification tasks based on EEG signals.

However, this study has certain limitations. Although significant progress has been made in MI-BCI classification algorithms, a substantial gap remains compared to the biological mechanisms of the brain. While this study focused on the alpha and beta bands, which are most relevant to motor imagery, it did not fully consider the characteristics of other frequency bands that are also crucial for EEG signal processing and could provide more detailed information about brain activity. Neglecting these features may limit a comprehensive understanding of EEG signals. Furthermore, most existing literature and open datasets focus on studies involving healthy individuals, with relatively few focusing on MI in patients. While this paper attempted an analysis of MI based on data from acute stroke patients, space limitations prevented us from delving deeply into brain network analysis. Future research could proceed in the following directions. First, expanding the frequency domain analysis to include more frequency bands could enable the construction of multi-frequency brain networks, thereby improving classification performance. Furthermore, future MI-BCI systems could incorporate the hierarchical structure of the brain, sparse connections between neurons, and parallel processing to build neural networks that better resemble human brain functions. For example, spiking neural networks (SNNs) could be developed to simulate information transmission between neurons [58]. By mimicking the structure and information processing methods of the brain, MI-BCI systems could achieve higher accuracy and efficiency, expanding their potential applications in fields such as medical rehabilitation. Additionally, it is necessary to collect more patient data, particularly EEG data from individuals with motor function disorders, to evaluate the applicability of the method across various conditions. Finally, conducting an in-depth analysis of brain networks in these patients is essential for investigating the interactions between different brain regions, allowing for a more comprehensive understanding of brain activity patterns during motor imagery.

REFERENCES

[1] X. Gao, Y. Wang, X. Chen and S. Gao, "Interface, interaction, and intelligence in generalized brain–computer interfaces," *Trends Cognit. Sci*, vol. 25, no. 8, pp. 671-684, 2021.

[2] J. Wolpaw and E. W. Wolpaw, *Brain-Computer Interfaces: Principles and Practice* Oxford, U.K.: OUP USA, 2012.

[3] H. Altaheri, G. Muhammad, M. Alsulaiman, S. Amin, G. Altuwaijri, W. Abdul, M. Bencherif and M. Faisal, "Deep learning techniques for classification of electroencephalogram (EEG) motor imagery (MI) signals: A review," *Neural Comput Appl*, vol. 35, no. 20, pp. 14681-14722, 2023.

[4] X. Zhang, L. Yao, X. Wang, J. Monaghan, D. Mcalpine and Y. Zhang, "A survey on deep learning-based non-invasive brain signals: recent advances and new frontiers," *J Neural Eng*, vol. 18, no. 3, pp. 031002, 2021.

[5] X. Tang, H. Shen, S. Zhao, N. Li and J. Liu, "Flexible brain–computer interfaces," *Nature Electronics*, vol. 6, no. 2, pp. 109-118, 2023.

[6] S. Aggarwal and N. Chugh, "Review of machine learning techniques for EEG based brain computer interface," *Arch Comput Methods Eng*, vol. 29, no. 5, pp. 3001-3020, 2022.

[7] N. Naseer and K. Hong, "fNIRS-based brain-computer interfaces: a review," *Front Hum Neurosci*, vol. 9, pp. 3, 2015.

[8] N. Logothetis, J. Pauls, M. Augath, T. Trinath and A. Oeltermann, "Neurophysiological investigation of the basis of the fMRI signal," *Nature*, vol. 412, no. 6843, pp. 150-157, 2001.

[9] Z. Tang, H. Yu, C. Lu, P. Liu and X. Jin, "Single-trial classification of different movements on one arm based on ERD/ERS and corticomuscular coherence," *IEEE Access*, vol. 7, pp. 128185-128197, 2019.

[10] A. Craik, Y. He and J. Contreras-Vidal, "Deep learning for electroencephalogram (EEG) classification tasks: a review," *J Neural Eng*, vol. 16, no. 3, pp. 031001, 2019.

[11] N. Padfield, J. Zabalza, H. Zhao, V. Masero and J. Ren, "EEG-based brain-computer interfaces using motor-imagery: Techniques and challenges," *Sensors*, vol. 19, no. 6, pp. 1423, 2019.

[12] Z. Gao, W. Dang, X. Wang, X. Hong, L. Hou, K. Ma and M. Perc, "Complex networks and deep learning for EEG signal analysis," *Cogn Neurodyn*, vol. 15, no. 3, pp. 369-388, 2021.

[13] R. Fu, Y. Du, S. Wang, G. Wen, J. Chen, and Y. Li, "Dynamical Differential Covariance Based Brain Network for Motor Intent Recognition," *IEEE Sens J*, vol. 24, no. 5, pp. 6515–6522, Mar. 2024.

[14] J. Gonzalez-Astudillo, T. Cattai, G. Bassignana, M. Corsi and F. Fallani, "Network-based brain–computer interfaces: principles and applications," *J Neural Eng*, vol. 18, no. 1, pp. 011001, 2021.

[15] Y. Hou, S. Jia, X. Lun, Z. Hao, Y. Shi, Y. Li, R. Zeng and J. Lv, "GCNs-net: a graph convolutional neural network approach for decoding time-resolved eeg motor imagery signals," *IEEE Trans Neural Netw Learn Syst*, 2022.

[16] Y. Miao, J. Jin, I. Daly, C. Zuo, X. Wang, A. Cichocki and T. Jung. "Learning common time-frequency-spatial patterns for motor imagery classification," *IEEE Trans Neural Syst Rehabil Eng*, vol. 29, pp. 699-707, 2021.

[17] N. Malan and S. Sharma, "Feature selection using regularized neighbourhood component analysis to enhance the classification performance of motor imagery signals," *Comput Biol Med*, vol. 107, pp. 118-126, 2019.

[18] F. Wu, A. Gong, H. Li, L. Zhao, W. Zhang and Y. Fu, "A new subject-specific discriminative and multi-scale filter bank tangent space mapping method for recognition of multiclass motor imagery," *Front Hum Neurosci*, vol. 15, pp. 595723, 2021.

[19] Y. Hou, T. Chen, X. Lun and F. Wang, "A novel method for classification of multi-class motor imagery tasks based on feature fusion," *Neurosci Res*, vol. 176, pp. 40-48, 2022.

[20] M. Kabir, S. Mahmood, A. Al Shiam, A. Musa Miah, J. Shin and M. Molla, "Investigating feature selection techniques to enhance the performance of EEG-based motor imagery tasks classification," *Mathematics*, vol. 11, no. 8, pp, 1921, 2023.

[21] S. Bandi, S. Sreeja and A. Bablani, "Classification of Motor Imagery based EEG signals using Ensemble model," in*proc. IEEE International Conference for Innovation in Technology*, 2024, pp. 1-6.

[22] H. Yang, F. Wu, N. Zhang, C. Chen, A. Wei, F. Peng and Z. Li, "A Transfer Learning Method for Motor Imagery EEG Signals Classification Based on CCSP and Riemannian Tangent Space Mapping," in *proc. IEEE International Conference on Real-time Computing and Robotics*, 2023. pp. 707-712.

[23] R. Schirrmeister et al., "Deep learning with convolutional neural networks for EEG decoding and visualization," *Hum Brain Mapp*, vol. 38, no. 11, pp. 5391—5420, 2017.

[24] V. Lawhern et al., "EEGNet: a compact convolutional neural network for EEG-based brain-computer interfaces," *J Neural Eng*, vol. 15, no. 5, pp. 056013, 2018.

[25] H. Altaheri, G. Muhammad and M. Alsulaiman, "Dynamic convolution with multilevel attention for EEG-based motor imagery decoding," *IEEE Internet Things J*, 2023.

[26] J. Hwang, S. Park and J. Chi, "Improving multi-class motor imagery EEG classification using overlapping sliding window and deep learning model," *Electronics*, vol. 12, no. 5, pp. 1186, 2023.

[27] Z. Jia, Y. Lin, J. Wang, K. Yang, T. Liu, and X. Zhang, "MMCNN: A multi-branch multi-scale convolutional neural network for motor imagery classification," in *Machine Learning and Knowledge Discovery in Databases*, F. Hutter, K. Kersting, J. Lijffijt, and I. Valera, Eds. Cham, Switzerland: Springer, 2021, pp. 736–751.

[28] Y. Hou, L. Zhou, S. Jia and X. Lun, "A novel approach of decoding EEG four-class motor imagery tasks via scout ESI and CNN," *J Neural Eng*, vol. 17, no. 1, pp. 016048, 2022.

[29] H. Dose, S. Jakob, H. Iversen and S. Puthusserypady, "An end-to-end deep learning approach to MI-EEG signal classification for BCIs," *Expert Syst Appl*, vol. 114, pp. 532-542, 2018.

[30] J. Yang, S. Yao and J. Wang, "Deep fusion feature learning network for MI-EEG classification," *Ieee Access*, vol. 6, pp. 79050-79059, 2018.

[31] H. Li, M. Ding, R. Zhang and C. Xiu, "Motor imagery EEG classification algorithm based on CNN-LSTM feature fusion network," *Biomed Signal Process Control*, vol. 71, pp. 103342, 2022.

[32] W. Zhang, V. Muravina, R. Azencott and Z. Chu, "Mutual information better quantifies brain network architecture in children with epilepsy," *Comput Math Methods Med*, vol. 2018, pp. 6142898, 2018.

[33] C. Sun, F. Yang and C. Wang et al., "Mutual information-based brain network analysis in post-stroke patients with different levels of depression," *Front Hum Neurosci*, vol. 12, no. 1, pp. 285, 2018.

[34] M. Ma, X. Wei and Y. Cheng et al., "Spatiotemporal evolution of epileptic seizure based on mutual information and dynamic brain network," *BMC Med Inform Decis Mak*, vol. 21, no. Suppl 2, pp. 80, 2021.

[35] Z. Wang, Z. Zhou and Y. He et al., "Functional integration and separation of brain network based on phase locking value during emotion processing," *IEEE T COGN DEV SYST*, vol. 15, no. 2, pp. 444-453, 2020.

[36] Y. Zhang, G. Yan and W. Chang et al., "EEG-based multi-frequency band functional connectivity analysis and the application of spatio-temporal features in emotion recognition," *Biomed Signal Process Control*, vol. 79, pp. 104157, 2023.

[37] G. Cui, X. Li and H. Touyama et al., "Emotion recognition based on group phase locking value using convolutional neural network," *Sci Rep*, vol. 13, no. 1, pp. 3769, 2023.

[38] H. Polat, "Brain functional connectivity based on phase lag index of electroencephalography for automated diagnosis of schizophrenia using residual neural networks," *J Appl Clin Med Phys*, vol. 24, no. 7, pp. e14039, 2023.

[39] T. Song, W. Zheng, P. Song and Z. Cui, "EEG emotion recognition using dynamical graph convolutional neural networks," *IEEE Trans Affect Comput*, vol. 11, no. 3, pp. 532-541, 2018.

[40] L. Zhang, L. Wang, D. Zhu et al., "Predicting brain structural network using functional connectivity," *Med Image Anal*, Vol. 79, pp. 102463, 2022.

[41] Y. Hou, S. Jia and X. Lun et al., "Deep feature mining via the attention-based bidirectional long short term memory graph convolutional neural network for human motor imagery recognition," *Front Bioeng Biotechnol*, vol. 9, pp. 706229, 2022.

[42] Z. Wang, Y. Tong, and X. Heng, "Phase-locking value based graph convolutional neural networks for emotion recognition," *IEEE Access*, vol. 7, pp. 93711-93722, 2019.

[43] J. Lachaux, E. Rodriguez and J. Martinerie et al., "Measuring phase synchrony in brain signals," *Hum Brain Mapp*,vol. 8, no. 4, pp. 194-208, 1999.

[44] C. Stam, G. Nolte and A. Daffertshofer, "Phase lag index: assessment of functional connectivity from multi channel EEG and MEG with diminished bias from common sources," *Hum Brain Mapp*, vol. 28, no. 11, pp. 1178-1193, 2007.

[45] G. Niso et al., "HERMES: towards an integrated toolbox to characterize functional and effective brain connectivity," *Neuroinformatics*, vol. 11, pp. 405-434, 2013.

[46] G. Nolte et al., "Robustly estimating the flow direction of information in complex physical systems," *Phys Rev Lett*, vol. 100, no. 23, pp. 234101, 2008.

[47] A. Goldberger, L. Amaral and L. Glass et al., "PhysioBank, PhysioToolkit, and PhysioNet: components of a new research resource for complex physiologic signals," *Circulation*, vol. 101, no. 23, pp. e215-e220, 2000.

[48] H. Cho, M. Ahn and M. Kwon, "EEG datasets for motor imagery brain–computer interface," *GigaScience*, vol. 6, no. 7, pp. gix034, 2017.

[49] H. Liu, P. Wei and H. Wang et al., "An EEG motor imagery dataset for brain computer interface in acute stroke patients," *Sci Data*, vol. 11, no. 1, pp. 131, 2024.

[50] G. Pfurtscheller and F. H. Lopes da Silva, "Event-related EEG/MEG synchronization and desynchronization: Basic principles," *Clin. Neurophysiol*, vol. 110, no. 11, pp. 1842–1857, 1999.

[51] M. Xia, J. Wang and Y. He, "BrainNet Viewer: a network visualization tool for human brain connectomics," *PloS one*, vol. 8, no. 7, pp. e68910, 2013.

[52] L. Zayia and P. Tadi, "Neuroanatomy, motor neuron," 2020.

[53] Y. Li, L. Fan and H. Shen et al., "HR-SNN: An End-to-End Spiking Neural Network for Four-class Classification Motor Imagery Brain-Computer Interface," *IEEE Trans Cogn Dev Syst*, pp. 1-13, 2024.

[54] D. Li, P. Ortega and X. Wei et al., "Model-agnostic meta-learning for EEG motor imagery decoding in brain-computer-interfacing," in *proc. 2021 10th International IEEE/EMBS Conference on Neural Engineering (NER)*, pp. 527-530, 2021.

[55] Z. Fang, W. Wang and S. Ren, "Learning regional attention convolutional neural network for motion intention recognition based on EEG data," in *proc. IEEE Biomed. Circuits Syst. Conf. (BioCAS)*, pp. 1570–1576, Oct. 2021.

[56] X. Wang, M. Hersche, M. Magno, and L. Benini, "Mi-bminet: An efficient convolutional neural network for motor imagery brain–machine interfaces with eeg channel selection," in *IEEE SENS. J*, 2024.

[57] W. Huang, W. Chang and G. Yan et al., "Spatio-spectral feature classification combining 3D-convolutional neural networks with long short-term memory for motor movement/imagery," *Eng Appl Artif Intell*, Vol. 120, pp. 105862, 2023.

[58] Z. Yi, J. Lian, Q. Liu, H. Zhu, D. Liang, and J. Liu, "Learning rules in spiking neural networks: A survey," *Neurocomputing*, Vol. 531, pp. 163–179, Apr. 2023.